NASA Technical Memorandum 82934

Investigation of Wear Phenomena by Microscopy

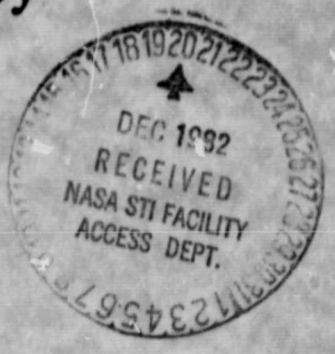

Donald H. Buckley
Lewis Research Center
Cleveland, Ohio

Prepared for the
Microscopy of the Degradation of Materials (Wear and Erosion),
MICRO 82, International Symposium and Exhibition
sponsored by the Royal Microscopical Society
London, England, July 12-16, 1982

NASA

INVESTIGATION OF WEAR PHENOMENA BY MICROSCOPY

by Donald H. Buckley

National Aeronautics and Space Administration
Lewis Research Center
Cleveland, Ohio 44135

ABSTRACT

This paper discusses the various wear mechanisms involved in the loss of material from metallic and nonmetallic surfaces. The results presented indicate how various microscopy techniques used in conjunction with other analytical tools can assist in the elucidation of a wear mechanism. Without question, microscopy is the single most important tool for the study of the wear of surfaces, to assess/address inherent mechanisms of the material removal process.

INTRODUCTION

Wear has been defined as, "the progressive loss of substance from the operating surface of a body occurring as a result of relative motion at the surface" (Friction, Wear and Lubrication GLOSSARY OF TERMS, 1969). Thus, the loss is a surface phenomenon which can be readily studied with the aid of surface tools including various microscopy techniques.

In the examination of worn or wearing surfaces in practical machine elements in order to identify the cause of wear and reduce it, assuming as is generally the case that the wear is detrimental, one must be able to identify the wear mechanism. Once the mechanism for material loss is identified, measures can generally be taken to reduce or eliminate the wear.

There are a number of mechanisms that the tribologists recognize as accounting for the loss of material from an operating surface. Rabinowicz (1965) defines these as adhesive, abrasive, corrosive and surface fatique. In addition, he recognizes as other forms of wear, fretting, erosion and cavitation.

In some machine elements small amounts of wear are detrimental. On the other hand, with some mechanical systems only a considerable amount of material loss contributes to the malfunctioning of individual components.

The usefulness of microscopy in the study of the wear of materials is continuously demonstrated. Godfrey (1980) and Buckley (1981) have reviewed the various wear mechanisms and presents micrographs in the process of mechanism identification. Engel (1976) has reviewed the impact wear of materials. American Society for Metals (1981), in a collection of recent papers, indicates the role of metallurgical principles in wear observations. Wear processes, monitoring and prevention are covered in a variety of papers presented in the Tribology Handbook (1973) Source Book on Wear Control Tech (1978) Wear (1979) Wear Control Handbook (1980), Fundamentals of Tribology (1980) and Wear of Materials (1977, 1979 and 1981). Microscopy techniques indicate the onset of wear, relationships to material properties, fatigue and fracture, temperature, velocity, and pressure effects. Polymers are widely used in practical tribological systems as coatings and understanding the manner and the mechanism by which they wear is extremely important. Significant advances in an understanding of polymer wear have been achieved through microscopy as evidenced by the collected works in Volumes 5A and 5B of Advances in Polymer Friction and Wear (1974) and by Evans and Lancaster (1979).

The objective of this paper is to review wear studies at NASA Lewis Research Center and demonstrate the importance of various microscopy techniques in the study of wear mechanisms. The mechanisms to be covered will include adhesive, abrasive, corrosive, fracture and fatigue, cavitation and erosive wear. The primary focus will be restricted to microscopy, although occasional reference will be made to other techniques for wear analysis. The latter will have to do primarily with elemental analysis.

WEAR MECHANISMS AND MICROSCOPE ANALYSIS

Adhesive Wear

When two solid surfaces are brought into contact in the atomically clean state, adhesion of one surface to the other nearly always occurs. On separation of the surfaces the interfacial bond is generally found to be stronger than the cohesive bonds in the cohesively weaker of the two materials. The result observed is that the cohesively weaker material transfers to the cohesively stronger and this constitutes adhesive wear. This same type of transfer can also occur for well lubricated surfaces by penetration of surface asperities through lubricating films.

The foregoing generalized statements concerning adhesive wear could not be made were it not for microscopic and energy dispersive X-ray spectroscopic observations. Adhesive transfer and wear at the fundamentalist of levels, namely the atomic, can be made with the field ion microscope with the atom probe attachment. This system allows both an atom-by-atom structural as well as elemental analysis.

Adhesion experiments are and have been conducted in the field ion microscope for direct observation of the adhesive transfer process. The apparatus used for these studies has been described by Brainard and Buckley (1971). Figure 1 is a field ion micrograph of a tungsten metal surface prior to adhesive contact. The micrograph reveals each and every atomic site on the solid metal surface and the circular rings the atomic planes.

Figure 2 presents the surface of figure 1 after having been contacted by a flat of polyimide polymer. The white spots present on the surface of figure 2 are polymer fragments of almost spherical shape with varying size. The metal surface is covered with polymer fragments. The interfacial metal to polymer adhesive bond is stronger than the cohesive bonds in the polymer and polymer transfer to metal is observed.

The strong adhesive bonding occurs not only for metals in contact with polymers but for metals in contact with metals as well. Figure 3 is a field ion micrograph of a tungsten surface after adhesive contact with gold. Clusters of the gold atoms about each tungsten were observed on the surface. Again, adhesive interfacial bonding is stronger than the cohesive bonding of the cohesively weaker metal, in this case the gold. The micrograph reveals a surface compound of the structure WAu_3. This compound found on the surface with field ion microscopy does not exist for bulk materials and cannot be found in phase diagrams.

Diamond is a broadly used industrial material. It is used in cutting, grinding, drilling and polishing. Understanding the surface interactions of diamond with metals is important to the understanding of why, for example, diamond wheels become charged in industrial grinding processes.

Simple sliding friction experiments with elemental metals in contact with diamond reveal that strong adhesive interactions occur leading to adhesive wear of metals and the charging of diamond surfaces with metal. Figure 4 is a replication electron micrograph of a wear track on a diamond surface after a single pass of a titanium rider across the surface. The black area in the center of the micrograph represents transferred titanium. The presence of the titanium is confirmed in the energy dispersive X-ray profile of figure 5. The profile was taken in the black area of figure 4. The copper in the profile of figure 5 comes from the mounting material.

From microscopic analysis of various metal surfaces of the transition series, a relationship between adhesive transfer and the d-valence bond character of the transition metals has developed. Miyoshi and Buckley (1981) have found this relationship to exist for these metals in contact with themselves, diamond, silicon carbide, boron nitride and manganese zinc ferrite.

Abrasive Wear

One of the most common types of wear by abrasion is that associated with the industrial process of grinding. The material removed is abrasively worn away. In dry grinding extremely high surface temperatures, 1000-1500° C and higher can readily be achieved. Such temperatures can have a pronounced effect on the nature of the wear observed.

Microscopic analysis of wear debris obtained in the abrasive wear process of grinding provides some interesting insight into the mechanism of wear. A fairly common wear particle found is one having a nearly uniform spherical shape. One such particle is presented in figure 6 which was taken from Jones (1976).

Figure 6(a) presents the spherical particle fractured revealing its hollow nature. Figure 6(b) indicates the spherical shape of the partical prior to fracture. The inside topography (Fig. 6(a)) reveals a surface character that could result from rapid cooling of a molten alloy.

From the analysis of debris such as that presented in figure 6, one can conclude that in the solid-state contact region localized surface melting occurs and the molten film contracts into a shape having the least surface area because of surface tension. This contraction process produces then the spherical wear particle.

The abrasive removal of material cannot only occur under conditions of intentional material removal such as in grinding but in well-lubricated systems where attempts are made to minimize wear. Dirt or wear debris which is hard relative to the lubricated surface may become trapped in the contact zone and cause abrasive loss of material from one or both of the contacting surfaces. This type of wear process is frequently observed in practical machinery. In recent years solids such as graphite, molybdenum disulfide

and teflon have been added to oils with the intent of reducing wear. They are generally considered to be very good solid lubricants and their presence in the oil is to act as anti-wear additives. In some instances, however, these materials which are supposed to reduce wear will actually increase it. This phenomenon has been demonstrated by Cusano and Sliney (1982) with both graphite and molybdenum disulfide added to oils.

Figure 7 presents wear scars generated on a steel ball in sliding contact with a glass plate. A light optical microscope was used to view the zone of contact between ball and plate by viewing with the microscope through the plate. Both ball and disk can be driven to achieve rolling contact, sliding or a combination of rolling and sliding.

The upper left-hand photograph of figure 7 represents the surface condition for sliding with oil. The remaining photographs represent sliding conditions for the oil containing molybdenum disulfide with various size MoS_2 particles some in suspension. Abrasive wear scars can be seen on all of the surfaces where molybdenum disulfide has been added to the oil. The edges of the hexagonal layer lamellar solid have acted as micro-cutting tools to produce abrasive wear of the steel ball.

Corrosive Wear

The mechanical activity of the rubbing, rolling or sliding of two solids in contact supplies energy at the interface. In a corrosive media this energy can initiate or accelerate corrosive reactions. While the noncontacted region of a surface may show no signs of corrosive attack, the area in the contact region may exhibit considerable evidence of reactivity. Corrosive wear may be experienced in acidic or basic media. It can, however, also be seen on well-lubricated surfaces where an anti- or some other wear additive

in an oil reacts excessively with the surfaces or where environmental constituents cause excessive breakdown of the oil additives in the contact region.

Figure 8 presents micrographs of the wear surface on an iron surface which had been rubbed by aluminum oxide in a 0.001 N NaOH aqueous solution. The wear surface is shown with ordinary optical microscopy in figure 8(a). That same wear track is presented using SEM with the secondary-electron mode in figure 8(b) and in the backscattering mode in figure 8(c).

In the actual wear track generated on the iron surface as a result of sliding a very thick surface film forms. This film, with increased sliding, blisters and develops cracks. One such crack is seen in SEM micrograph of figure 8(d). X-ray photoelectron spectroscopy (XPS) analysis of the film seen in figure 8(d) reveals it to be ferric oxide (Fe_2O_3).

It is of interest to note that simple changes in the concentration of a corrosive substance on a solid surface can markedly alter wear behavior. For example, with iron small concentrations of NaOH (e.g., 0.001 and 0.01 N) accelerates the surface wear from that observed in water, as indicated in the surface profile traces of figure 9. Rengstorff, Miyoshi, and Buckley, (1982) have, however, observed that when the concentration of NaOH is increased to 20 N a noticeable decrease in wear occurs as indicated in figure 9. The wear is less than that observed in water. The wear decrease is accompanied by a decrease in friction as indicated in figure 9 and surface analysis with XPS reveals a decrease in the surface concentration of Fe_2O_3.

Fracture and Fatigue

In practical tribological systems surfaces such as those of bearing and gear surfaces are very highly loaded in the contact region. These loads produce considerable stress both surface and sub-surface. With relatively

brittle materials these stresses even generate cracks in the material which will lead to fracture and the formation of wear particles.

Sliney (1976) has viewed the contact region of a steel ball in contact with a boron silicate glass plate by viewing the contact region with light optical microscopy through the glass plate. With a normal load applied to the ball, the contact is, of course, under a compressive stress component perpendicular to the direction of sliding. Additionally, it has been shown that the tangential stress generated by friction creates a compressive stress component parallel to the sliding direction ahead of the contact and a corresponding tensile stress component in the wake of the contact. The location of stress reversal depends upon the friction. For a friction coefficient of 0.33, as an example, the reversal from compressive to tensile stress occurs within the contact at about one-sixth of the contact diameter from the exit and the maximum tensile stress is at the exit. The stress reversal phenomenon is an important factor in the formation and propagation of surface cracks. This has been reported by others and was also experimentally observed in our study.

Figure 10 shows a series of nearly identical cracks in the glass passing through the concentrated contact. In figure 10(a), a crack is barely visible at the center of the contact where the surface is under compression. In figure 10(b), the same crack has moved near the exit where the surface is under tension and the crack has widened and has propagated laterally.

Figure 10(c) is a plot of surface stress components within the contacts and in the sliding direction. Although friction was not measured in these experiments, it is clear that crack closing under compression and widening under tension qualitatively agree with the analysis.

Fatigue is a mechanism of wear for mechanical components and to study this phenomenon accelerated testing is frequently employed. During the course of such studies the nature of the wear process is closely observed. In such studies spherical wear particles are frequently observed to form. The particles are similar to those observed in figure 6 with the abrasive wear process of grinding, although the mechanism for their formation may be entirely different.

Figure 11(a) is a micrograph of a fatigue wear particle and figure 11(b) is an X-ray analysis of the sphere revealing the material to be of the same composition as that of the bearing surface from which it came (Jones, 1981).

Cavitation

The most important mechanism of liquid erosion involves the generation of bubbles in the liquid and their subsequent damaging collapse. This fluid-dynamic process is called cavitation and resulting material removal is called cavitation erosion or wear. Both optical and electron microscopy have been extremely beneficial in the study of cavitation damage as reported in the book by (Knapp et al. 1970, Hammitt 1980) and in several papers in special technical publications of the American Society for Testing and Materials (1967, 1970, 1974, 1979), in erosion (1978), and in erosion by solid and liquid impact (1979). Erosion by liquid impact has been discussed in detail by Springer (1976). Although there are several excellant papers in prestigeous journals it is very difficult to refer to each and everyone in this limited space.

Microscopic studies of eroded surfaces by cavitation reveal a roughened topography. Examination of the wear debris indicates that in some instances spherical wear particles (Fig. 12(a)) are observed to be generated analgous to that seen in grinding and fatigue (Figs. 6 and 11).

Figures 12(b) and (c) present flow of material and erosion debris under cavitation erosion conditions. It is obvious that erosion debris is different under different experimental conditions.

Erosion

Erosion by the impingement of abrasive particles against a solid surface is a form of abrasive wear (Rabinowicz, 1979). It follows that all the four forms of wear (adhesion, abrasion, corrosion and surface fracture) can manifest themselves in eroding systems.

Solid impingement erosion as a mechanism for the loss of material from the surface of solids has taken on considerable significance in recent years. It has practical implications in jet aircraft engine ingestion and coal gasification processes.

A detailed examination of the erosive wear process indicates a number of interesting phenomena. For example, erosion can and will contain several mechanisms of wear.

Salik and Brainard (1979) used a single spherical particle impact device and retrieved the impinging particle for surface analysis. Scanning electron microscopy (SEM) coupled with X-ray dispersive energy analysis of the spherical steel ball revealed that a considerable amount of the material lost from the eroded surface had been transferred by adhesion to the eroding particle. In fact, for steel spheres impinging on an aluminum alloy surface, a part of the loss was due to adhesive transfer of aluminum to the steel.

A surface of a steel ball is shown schematically in figure 13. Nearly one-half of the ball surface is covered by a thin film of transferred aluminum after impact. In addition, localized chunks of material are observed in the transfer zone. Figure 14(a) presents an SEM of the region called out in figure 13 as well as X-ray emission spectra. In figure 14(b) the upper

half of the ball is analyzed and in figure 14(c) the lower half. Mapping of a typical ball surface reveals the transfer shown in figure 13 which accounted for the major portion of material removal from the aluminum alloy's surface by impingement.

The erosion process can produce marked metallurgical changes in the surface layers of materials. Both surface work hardening and microcrystallization have been observed.

Metallurgical transformations are observed on the surfaces of the multiple erodant materials. The erodant particle shape is seen to effect loss and alter topography. Further, there is an incubation period prior to the initiation of material loss and impingement pressure or velocity is directly related to cumulative erosive loss.

Table I indicates the erosive loss of an aluminum alloy by the impingement of glass beads as a function of surface pre-treatment. Despite the nature of the surface mechanical pre-treatment the weight loss was approximately the same. Similar observations of the effect of prior cold work on erosion were also reported by Finnie et al. (1967). The reason for the likeness in erosive wear can be seen with the aid of the micrograph of figure 15. This cross-section of the erosive crater bottom is representative of what was obtained with various pre-treatments after impact. The surface recrystallizes and a work hardened layer develops at the surface of the bulk material. This composition develops very early and as a result thereof the wear is approximately the same because the surface exposed to erosion is approximately the same.

Table II presents erosion data for the erosion of three aluminum single crystal surfaces of different orientation. Despite differences in orientation and accordingly atomic density, weight loss is again nearly the same.

X-ray Laue patterns from one of the single crystal surfaces (110) both before and after erosion are presented in figure 16. The ring structures present in the X-ray diffraction pattern of figure 16(b) reflect the presence of a polycrystalline surface layer demonstrating possible recrystallization.

Erosion studies have been conducted by Rao, Young, and Buckley (1982a) with aluminum surfaces eroded by both glass beads and crushed glass. Some unusual surface profiles have been observed with SEM.

Figure 17(a) shows a photograph of an aluminum specimen after having been exposed to glass beads for 20 minutes at 0.41 MPa argon driving gas pressure. Figure 17(b) is a surface profile of the same specimen. The specimen, photographed at an advanced stage of erosion, shows a damage pattern which appears to be divided into five distinct regions.

Region 1 consists mainly of radial deformation tracks, emanating from the center of the impact crater. The depth and width of the tracks increase with radial distance from the center of the pit. Specimens observed during the earliest phases of erosion do not show any indication of these radial patterns.

Region 2 consists of both radial tracks and concentric rings, with the concentric rings overlapping the radial tracks. For convenience, these are called "radial-concentric" rings. This is believed to be the first observation of such patterns. The surface profiles (fig. 17(b)) indicate that region 2 has a very steep slope. The rings consist of small steps of 10 to 25 micrometers with wave-type circular crests inside the steep slopes of the pit. During the initial phases, only radial tracks are observed; the radial-concentric rings form later. When radial-concentric rings form, the distance between rings is larger than the width of the radial tracks.

Region 3 is also a steep-slope region (less steeper than region 2) comprised principally of radial tracks. The tracks are wider than the average size of the erodant particles. It was observed that the width of region 3 decreases with exposure time.

Region 4 is a very rough surface (compared to other regions) with irregular concentric, ripple and crest patterns. The slope is slight (from 1/100 to 1/500) and the wave-length between ripples varies between 10 and 25 micrometers.

Region 5 consists of a transition from the undamaged zone to the incipient erosion zone. Random pits are observed which appear to have been caused by both single as well as multiple impacts.

Figure 18 consists of of SEM micrograph of aluminum specimen examined at 0.54 MPa (gage) pressure and at 20 minutes exposure time. Several investigators (e.g. Finnie and Kabil, 1965; Sheldon and Finnie 1966; Carter et al. 1981) have described ripple formation at oblique impact angles. However, the ring patterns observed in the current study which result from normal impact (especially in region 2) have not been reported before. The present study shows that the intensity of erosion (impact pressure) plays a decisive role on the rate of development of the damage patterns and that the same type of patterns appear with different driving-gas pressures (hence, velocities).

Figure 19 is a cross-cut through the pit of the specimen exposed to glass bead erosion at 0.54 MPa for 20 minutes (the same specimen as shown in fig. 18. The lower photograph shows the entire pit at a magnification of approximately 15 times magnification. Evenly-spaced wave-crests of radial tracks can be seen in the magnified view of the bottom and more widely separated, deformed crests of the concentric rings can be seen in the magnified

view on the top right. A form of undercutting is observed. Considerable additional study and experimentation is needed to explain and understand the active mechanisms which give rise to the formation of these unusual patterns.

Figures 20(a) and (b) show SEM micrographs of glass beads before and after impact. Most of the erodant particles were originally thought to break up during impact. However, in the present investigation the samples of glass beads collected after impact at various time intervals reveal that a majority of the particles are not damaged (fig. 20(b)).

A SEM Energy Dispersive X-ray Spectroscopy (EDS) analysis was made of the glass beads before and after use as erodant particles. For the impact pressure used in this study, there was no indication of any aluminum adhering to the particle surfaces (within the sensitivity of the EDS facility). However earlier studies (Brainard and Salik, 1980) with angular particles showed material transfer. During the induction and acceleration periods aluminum surfaces showed many embedded glass beads. A typical energy dispersive X-ray emission spectrum of an aluminum surface during the acceleration period is shown in figure 20(c). The silicon and calcium peaks indicate the presence of glass bead traces on the surface of the aluminum specimen. As the damage progresses and transforms into erosion, the embedded glass beads are carried away by the inflowing and outflowing fluxes, and fewer remain on the specimen surface. The silicon/aluminum peak ratio drops from 0.198 at 1 minute to about 0.019 after 40 minutes. Fragmentation of particles may possibly take place at higher impact velocities, but this has not been observed. Further studies are necessary to understand (a) the reasons for the embedment of particles at early stages of erosion and their influence on the physics of the erosion process, (b) material removal mechanisms during the induction period, and (c) effects of high-impact velocity on the fragmentation of erodant particles.

The unusual patterns observed (figs. 17(a) and 18) on the specimen surfaces in these experiments are of particular interest in that they are created by glass sphere impact and the resulting deformation wear only. The cutting aspect of wear is believed to be nearly absent because the glass beads were not fractured after impact.

From the radial and concentric patterns observed on ductile materials from normal impact of glass beads, the following progressive development of erosion is postulated (see fig. 21). The impacting particles cause cyclic compression at the center of impact on the initially flat surface (fig. 21(a)). It is possible that a certain amount of local plastic deformation occurs even for low-velocity impact followed by beads being forced out of the impact areas. Figures 21(b) and (c) show the compression of material and pit deepening.

The outflow of glass beads is considered to be responsible for the initiation of small ripples away from the pit, probably associated with shear. As the exposure time increases the pits deepen and cause outflowing beads to be thrown away from the surface at an angle which is visualized in figures 21(e) and (f). The streams of erodant particles moving out of the pits are considered to be responsible for the initiation of radial tracks in regions 1 to 3 as well as the deepening and broadening of the pit. On further deepening of the pit, as indicated in figure 21(f), radial-concentric rings form since the momentum of the impacting jet has to be almost reversed in order for the particles to escape up the walls of the pit. Under these conditions, formation of a vortex flow might be taking place causing undercutting (see fig. 21(f)). Further work is in progress to more clearly understand the dynamics of the formation of these patterns.

Rao, Young, and Buckley (1982b) have studied the erosive wear of the plastic materials, polymethyl methacrylate (PMMA) polycarbonate (PC) and polytetrafluoroethylene (PTFE). These studies have been conducted in an analogous manner to the aluminum studies already described.

The damage patterns for all these polymers may be divided into four regions (Fig. 22). Region 1 is a central irregular pit surrounded by region 2, a nonuniform build-up of plastic material and glass where glass beads are the erodant. This region consists of peaks and valleys from 30 to 100 micrometers deep. Region 3 is a slightly raised region which slopes toward the original surface. Region 4 is a depressed area 5 to 10 micrometers below the original surface level.

Evidence for material build-up can be found in surface traces of PMMA and PC. These are believed to be due to heat distortion and/or partial melting and redeposition of material during impingement. A temperature rise as high as 190 C during impact conditions has been reported earlier by Neilson and Gilchrist (1968). Melting of metallic material surfaces have also been reported recently (e.g. Brown and Edington 1981 a,b) during spherical and angular particle impingement conditions. Also, increased levels of the glass bead material is observed in this area. Material build-up was neglible for PTFE. However, the surfaces of the PTFE specimens were observed to have changed color from white to light brown after glass bead impact. This color change is also believed to be due to heat generated during impingement. It is reasonable that teflon would be least affected by heat in view of its lower heat distortion temperature. Darkening of nylon and polypropylenol surfaces due to solid impingement was reported earlier by Tilly (1969) and has been attributed to a chemical change in the surface possibly associated with localized heating. Figure 22 shows SEM micrographs of an eroded PMMA specimen exposed to glass bead impingement for 15 seconds.

These micrographs show material build-up, a fissure between regions 2 and 3 (fig. 22(a)), and also layers or bands in some areas (fig. 23(b)). These bands are, in general, circumferential arcs surrounding the center of impact, with decreasing elevations away from the center of impact. These are believed to be formed by melting and resolidification of the plastic material. However, further studies are necessary to identify the mechanism(s) involved with the formation of these stratified layers.

The results of Rao, Young, and Buckley (1982) of PMMA, PC, and PTFE indicate reproducibility for the erosion process of plastic materials under normal impingement. The scatter of data increased with increased volume loss. PMMA erodes rapidly compared with PC and PTFE. PTFE is observed to be the most resistant of the three polymeric materials. The following discussion for the ranking of the erosion resistance of the tested materials is based on various properties of these materials. The erosion resistance varies directly with the ultimate elongation, strain energy and maximum service temperature and inversely with tensile strength, yield strength and modulus of elasticity of these polymers. No single property is clearly dominant in its effect on erosion resistance. It is believed, however, that some combination of high ultimate elongation, impact strength and maximum service temperature contributes to high erosion resistance. Many more materials with carefully measured properties need to be examined to draw any clear conclusions regarding material property correlations with erosion resistance. A previous investigation by Eyre (1976) has stated that natural and synthetic rubbers exhibit good erosion resistance due to their low modulus of elasticity, and some correlation exists with ultimate resilience [defined as (tensile strength)^2/modulus of elasticity]. The ultimate resilience for the polymers examined herein do not vary sufficiently to arrive at the same conclusion in this study.

CONCLUSIONS

There are a number of very specific and different mechanisms of wear recognized. These include adhesive, abrasive, corrosive, fatigue, fracture, cavitation and erosion. All of these forms of wear have distinct characteristic features which tend to set them apart from each other. Various microscopy techniques have been indispensable in the identification of wear mechanisms.

At the atomic level the field ion microscope used in conjunction with the atom probe gives both a structural and chemical analysis of adhesive transfer and accordingly wear on the basis of a single atom. The generation of wear particles having spherical shapes have been detected in abrasive, fatigue and cavitation wear with the assistance of scanning electron microscopy. Using optical microscopy for in-situ analysis of lubricated contacts reveals abrasive wear with materials previously thought to be solid lubricants.

The use of various microscopic techniques in conjunction with surface profilometry and X-ray photoelectron spectroscopy has provided detailed insight into the nature and action of corrosive wear. Microscopic analysis of surfaces under load has revealed the classical fracture behavior of brittle materials in loaded contacts.

Studies of erosive wear indicate that at the impacting surfaces adhesion can occur resulting in the adhesive transfer and accordingly wear of the surfaces and in certain instances material loss by the erosion process is dominated by adhesive transfer and wear. Microscopic sectional analysis of eroded surfaces reveal metallurgical transformations.

The erosion of metals by crushed glass and glass beads establishes distinct regions in the erosion pits associated with material loss. Material removal is directly related to impact velocity for aluminum surfaces.

With polymers, erosive wear of surfaces is found to contain again distinct regions and an incubation period before material loss commences. Of the three polymer structures, polymethyl methacrylate (PMMA) polycarbonate and polytetrafluoroethylene, (PTFE) the least amount of erosive wear was detected with PTFE and the greatest with PMMA. These losses can be related to other properties of the polymers.

REFERENCES

Advances in Polymer Friction and Wear)1974) Polymer Science and Technology, vols. 5A and 5B (Ed. by L. H. Lee), Plenum Press, New York.

American Society for Testing and Materials (1967, 1970, 1974, 1979). Special Technical publications 408, 474, 567 and 664, ASTM, Philadelphia, PA.

Brainard, W. A. & Buckley, D. H. (1971) Preliminary studies by field ion microscopy of adhesion of platinum and gold to tungsten and iridium, NASA TN D-6492, National Aeronautics and Space Administration, Washington, D.C.

Brainard, W. A. & Salik, J. (1980) Scanning-electron-microscope study of normal - impingement erosion of ductile metals. NASA TP-1609, National Aeronautics and Space Administration, Washington, D.C.

Brown, R. & Edington, J. W. (1981a) The melting of metal targets during erosion by hard particles. Wear 71, 113.

Brown, R. & Edington, J. W. (1981b) Occurrence of melting during the solid particle erosion of copper. Wear 73, 193.

Brown, R., Jun, E. J. & Edington, J. W. (1981) Erosion of α-Fe by spherical glass particles. Wear 70, 347.

Buckley, D. H. (1981) Surface Effects in Adhesion, Friction, Wear and Lubrication Tribology Series 5, p. 429. Elsevier, Amsterdam.

Carter, G., Nobes, M. J. & Arshak, K. I. (1980) The mechanism of ripple generation on sandblasted ductile solids. Wear 65, 151.

Cusano, E. & Sliney, H. E. (1982a) Dynamics of solid dispersions in oil during the lubrication of point contacts, Part I - Graphite. ASLE Trans. 25, 183.

Cusano, C. & Sliney, H. E. (1982b) Dynamics of solid dispersions in oil during lubrication of point contacts, Part II - Molybdenum Disulfide. ASLE Trans. 25, 190.

Engel, P. A. (1976) Impact Wear of Materials. Elsevier Scientific Publishing Co., Amsterdam.

Erosion (1978) Treatise on Materials Science and Technology, vol. 16 (Ed. by C. M. Preece), Academic Press, New York

Erosion by Liquid and Solid Impact (1979) Proc. 5th Intl. Conf., Cambridge, England.

Evans, D. C. and Lancaster, J. K. (1979) The wear of polymers. In.: Treatise on Materials Science and Technology, vol. 13 (Ed. by D. Scott), p. 86, Academic Press, Inc., New York.

Eyre, T. S. (1976) Wear characteristics of metals. Tribology Int. 9, 203.

Finnie, I. & Kabil, Y. H. (1965) On the formation of surface ripples during erosion. Wear 8, 60.

Finnie, I., Wolak, J. & Kabil, Y. (1967) Erosion of metals by solid particles. J. Materials 2, 682.

Friction, Wear and Lubrication: (Tribology Glossary (1969) Organization for Economic Cooperation and Development, Paris.

Fundamentals of Friction and Wear of Materials (1981) (Ed. by D. A. Rigney) American Society for Metals, Metals Park, Ohio.

Fundamentals of Tribology (1980) (Ed. by N. P. Suh & N. Saka) MIT Press, Cambridge, Mass.

Godfrey, D. (1980) Diagnosis of wear mechanisms. In: Wear Control Handbook, (Ed. by M. B. Patterson & W. O. Winter), p. 283. The American Society of Mechanical Engineers, New York.

Hammitt, F. G. (1980) Cavitation and Multiphase Flow Phenomena. McGraw-Hill Book Co., New York.

Jones, W. R., Jr. (1976) Spherical artifacts on ferrograms. Wear 37, 193 .

Jones, W. R., Jr. (1981) Elucidation of wear mechanisms by ferrographic analysis, NASA TM-82737, National Aeronautics and Space Administration, Washington, D.C.

Knapp, R. T., Daily, J. W. & Hammitt, F. G. (1970) Cavitation, McGraw-Hill Book Co., New York.

Miyoshi, K. & Buckley, D. H. (1981) Adhesion and friction of transition metals in contact with nonmetallic hard materials, NASA TM-82605, National Aeronautics and Space Administration, Washington, D.C.

Neilson, J. H. & Gilchrist, A. (1968) An experimental investigation into aspects of erosion in rocket motor tail nozzle. Wear 11, 123.

Rabinowicz, E. (1965) Friction and Wear of Materials. p. 113, John Wiley & Sons, Inc., New York.

Rabinowicz, E. (1979) The wear equation for erosion of metals by abrasive particles. In: Proc. 5th Int. Conf. on Erosion by Solid and Liquid Impact, p. 38-1, Cambridge, England.

Rao, P. V., Young, S. G. & Buckley, D. H. (1982a) Morphology of ductile metals eroded by spherical particle impingement at normal incidence, NASA E-1092.

Rao, P. V., Young, S. G. & Buckley, D. H. (1982b) Solid spherical glass particle impingement studies of plastic materials, NASA E-1122.

Rengstorff, G. W. P., Miyoshi, K. & Buckley, D. H. (1982) Friction and wear of iron in corrosive media, NASA TP-1985, National Aeronautics and Space Administration, Washington, D.C.

Salik, J. & Brainard, W. A. (1979) Adhesive material transfer in the erosion of an aluminum alloy, NASA TM-79165, National Aeronautics and Space Administration, Washington, D.C.

Sheldon, G. L. & Finnie, I. (1966) On the ductile behavior of nominally brittle materials during erosive cutting. J. Eng. for Ind. Trans. ASME, 88, 387.

Sliney, H. E. (1976) Dynamics of solid lubrication as observed by optical microscopy, NASA TM X-71880, National Aeronautics and Space Administration, Washington, D.C.

Source Book on Wear Control Technology (1978) (Ed. by D. A. Rigney & W. A. Glaeser), American Society for Metals, Metals Park, Ohio.

Springer, G. S. (1976) Erosion by Liquid Impact. Scripta Publishing Co., John Wiley & Sons, New York.

Tilly, G. P. (1969) Erosion caused by airborne particles. Wear 14, 63.

Tribology Handbook (1973) (Ed. by M. J. Neale), John Wiley & Sons, New York.

Wear (1979) Treatise on Materials Science and Technology, vol. 13 (Ed. by D. Scott), Academic Press, Inc., New York.

Wear Control Handbook (1980) (Ed. by M. B. Peterson & W. O. Winter), The American Society of Mechanical Engineers, New York.

Wear of Materials 1977 (Ed. by W. A. Glaeser, K. C. Ludema & S. K. Rhee); Wear of Materials 1979 (Ed. by K. C. Ludema, W. A. Glaeser & S. K. Rhee); Wear of Materials 1981 (Ed. S. K. Rhee, A. W. Ruff & K. C. Ludema), American Society of Mechanical Engineers, New York.

TABLE I. - SURFACE PROPERTIES AND EROSION OF 6061 ALLOY SUBJECTED TO VARIOUS MECHANICAL TREATMENTS

Surface treatment	Surface roughness, μm,	Microhardness, kg/mm^2	Weight loss on a 10-min erosion test, g
Annealed (baseline)	Variable	41	0.0410
Cold rolled	0.76	48	.0418
Ground	.37	50	.0405
Sand blasted	3.68	74	.0417
Glass bead blasted	2.29	76	.0412
Alundum blasted	4.06	110	.0414
Shot peened	Out of range	131	.0419

TABLE II. - EROSION OF Al SINGLE CRYSTALS

Orientation	Weight loss on a 2-min erosion test, g
(100)	0.0120
(110)	.0115
(111)	.0118

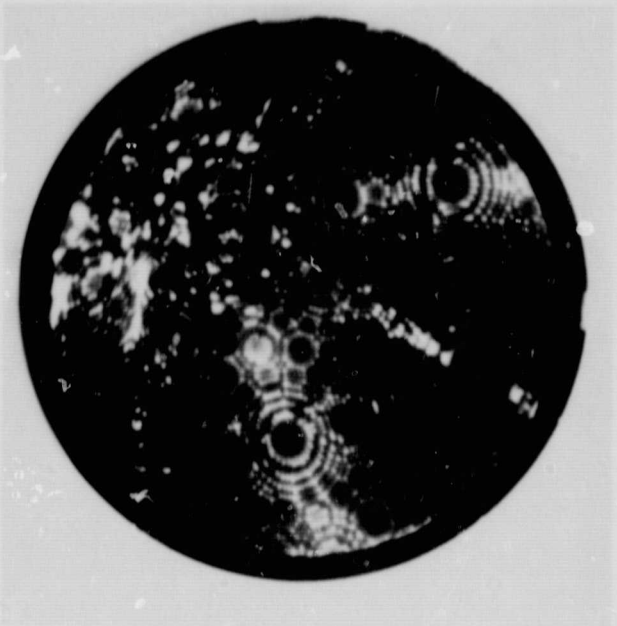

Figure 1. - Tungsten prior tc contact (15.0 kV, helium image gas, liquid nitrogen cooling).

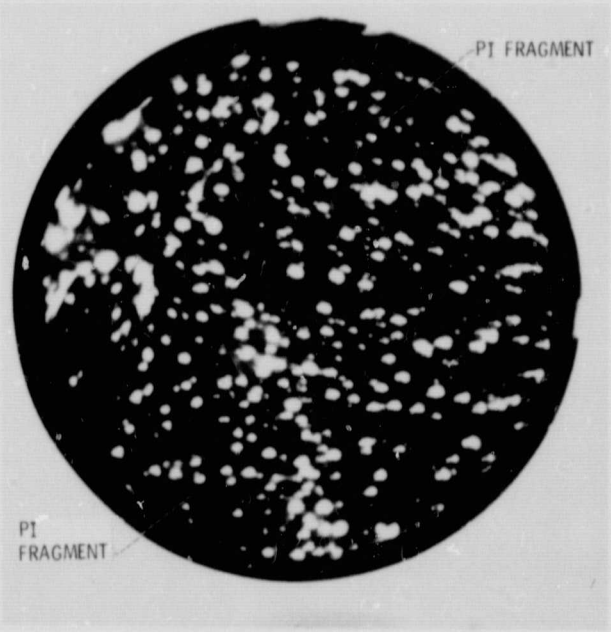

Figure 2. - Tungsten after polyimide contact (13.0 kV, helium image gas, liquid helium cooling).

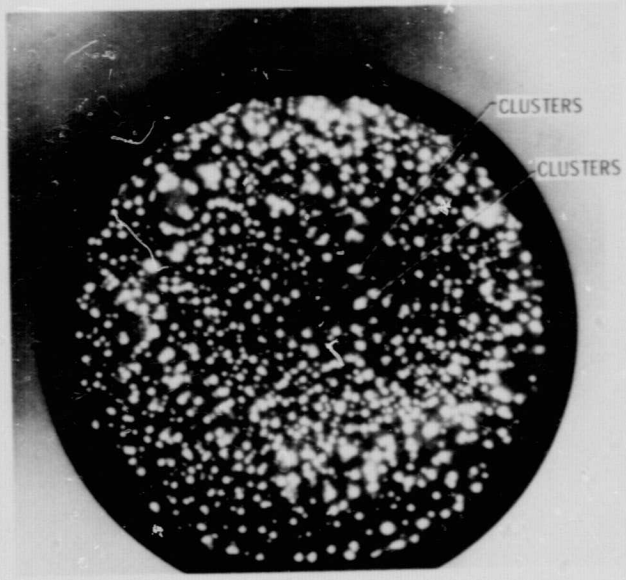

Figure 3. - Tungsten after gold contact at 13.0 kV with voltage raised to 14.5 kV for 30 sec; liquid-helium cooling.

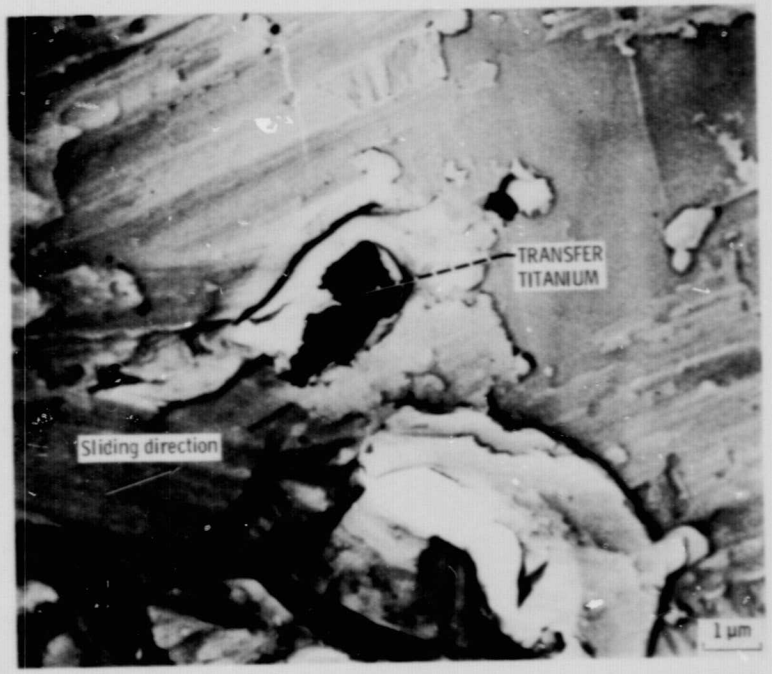

Figure 4. - Replication electron micrograph of wear track on {111} diamond surface. Single pass of titanium rider; sliding direction, $\langle 1\bar{1}0 \rangle$; sliding velocity, 3×10^{-3} m/min; load, 0.2 N; room temperature; vacuum pressure, 10^{-8} Pa.

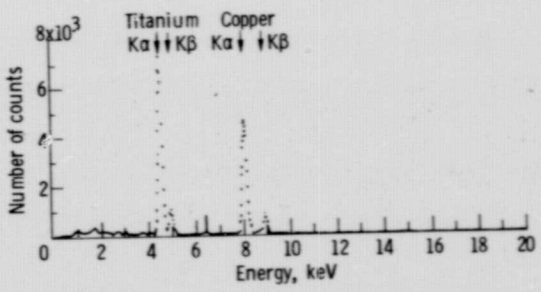

Figure 5. - Energy dispersive X-ray profile of a piece of wear debris.

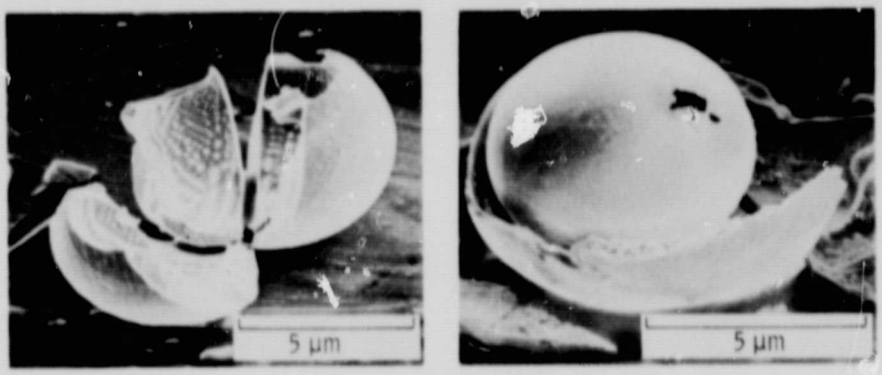

(a) Hallow nature of spherical particle. (b) Spherical debris.

Figure 6. - Scanning electron micrographs of spherical grinding debris.

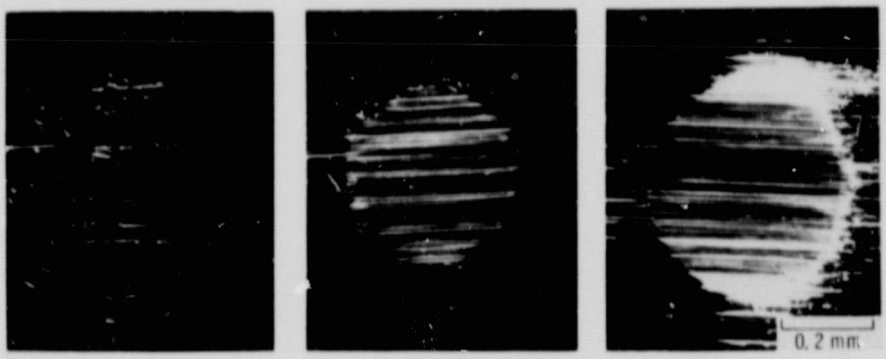

NO MoS_2 FINE MoS_2 COARSE MoS_2

CS-82-1389

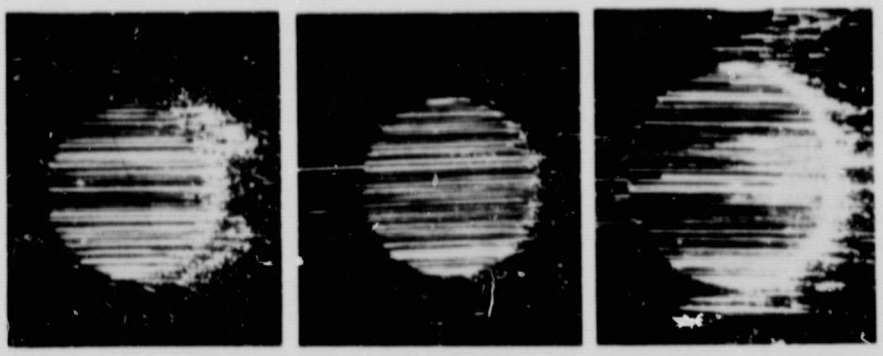

3% SUSPENSION GRADE MoS_2 3% MEDIUM GRADE MoS_2 3% COARSE GRADE MoS_2

CS-81-2289

Figure 7. - Effect of MoS_2 in 150 cS oil on abrasion of polished steel ball during sliding contact. 125X original magnification.

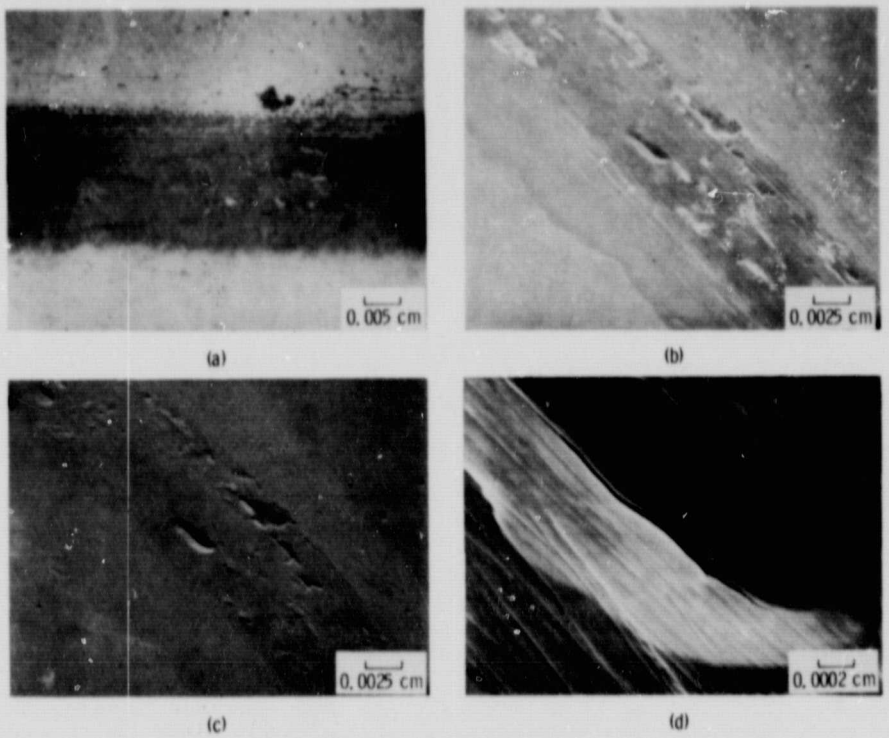

(a) Photomicrograph of wear track.

(b) SEM photograph of wear track, made with secondary-electron mode.

(c) SEM photograph of wear track, made with backscattering mode.

(d) SEM photograph of defect in center of (b) and (c), made with secondary-electron mode.

Figure 8. - Photomicrographs of wear track generated by Al_2O_3 ball sliding on iron flat in 0.001 N NaOH solution.

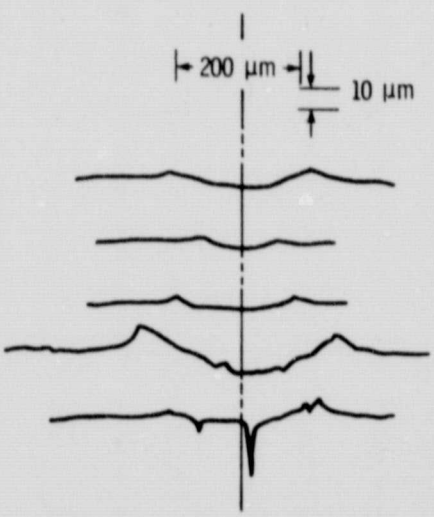

CORROSIVE MEDIUM	STATIC COEFFICIENT OF FRICTION, μ_s
H_2O	0.26
20 N NaOH	.17
0.4 N NaOH	.26
0.01 N NaOH	.52
0.001 N NaOH	.39

Figure 9. - Talysurf traverses across wear tracks generated by Al_2O_3 ball sliding on iron flat in various media. (Wear tracks were made on the iron flat.)

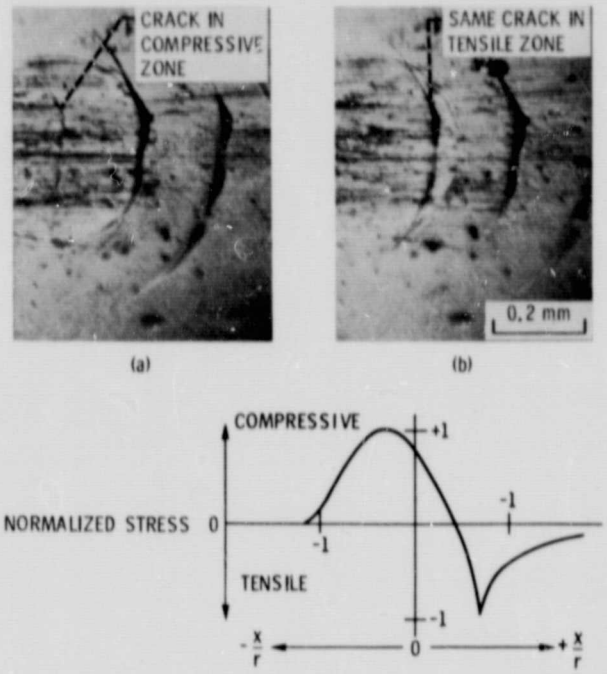

(a) Crack in compression.

(b) Crack in tension.

(c) Surface stress component in sliding direction.

Figure 10. - Crack formation and propagation in unlubricated contact. Load, 13.2 N (3 lb); original magnification, X150.

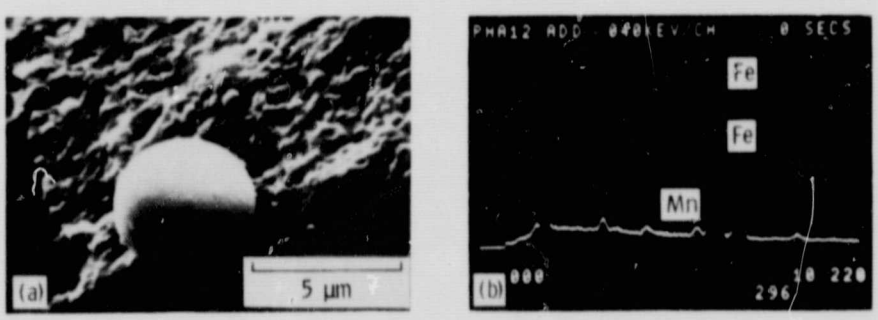

(a) Electron micrograph of spherical particle and friction polymer.

(b) EDAX of spherical particles.

Figure 11. - Wear particle from accelerated fatigue testing.

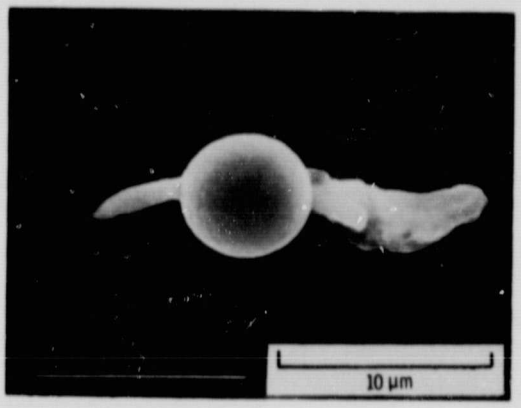

(a)

(a) Sphere produced by cavitation erosion.

Figure 12.

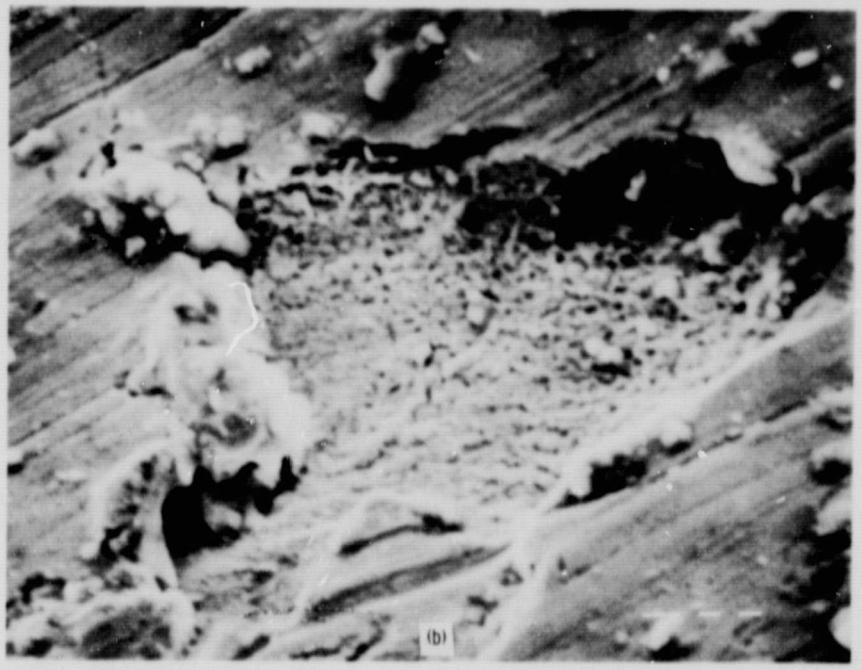

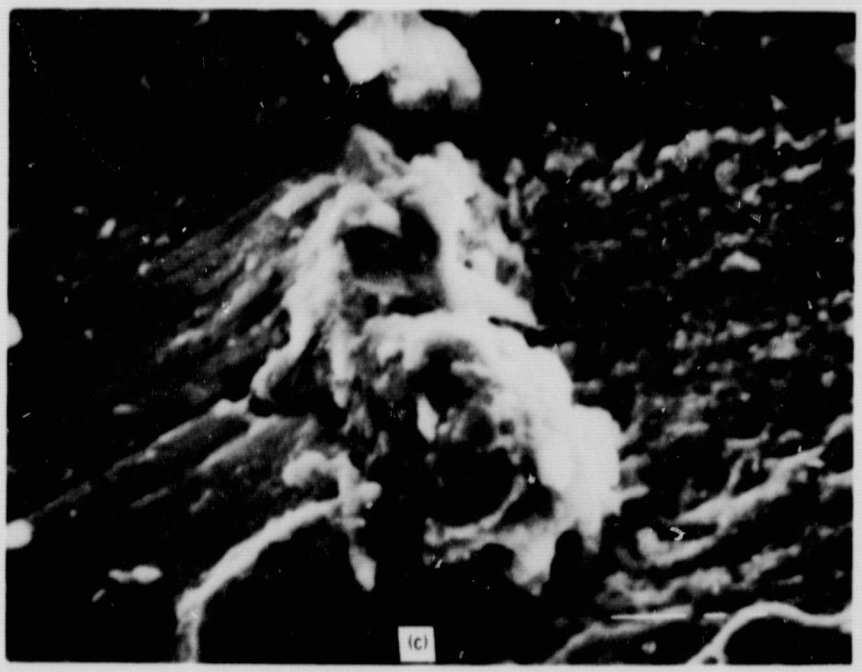

(b) Cavitation erosion pit on brass.

(c) Cavitation erosion pit showing flow of material.

Figure 12 - Concluded.

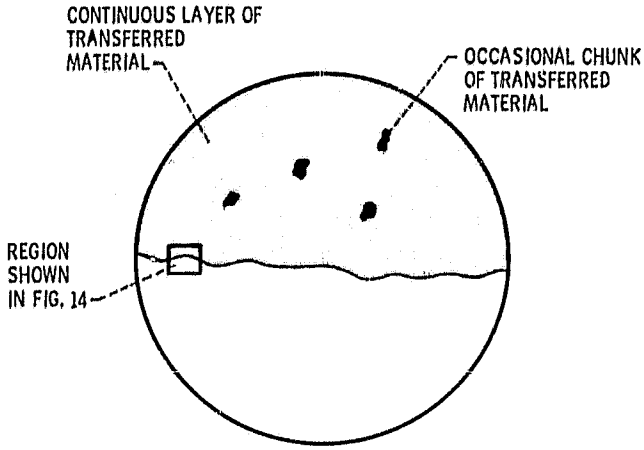

Figure 13. - Schematic illustration of steel ball surface after impinging on annealed 6061 aluminum surface at 180 m/sec.

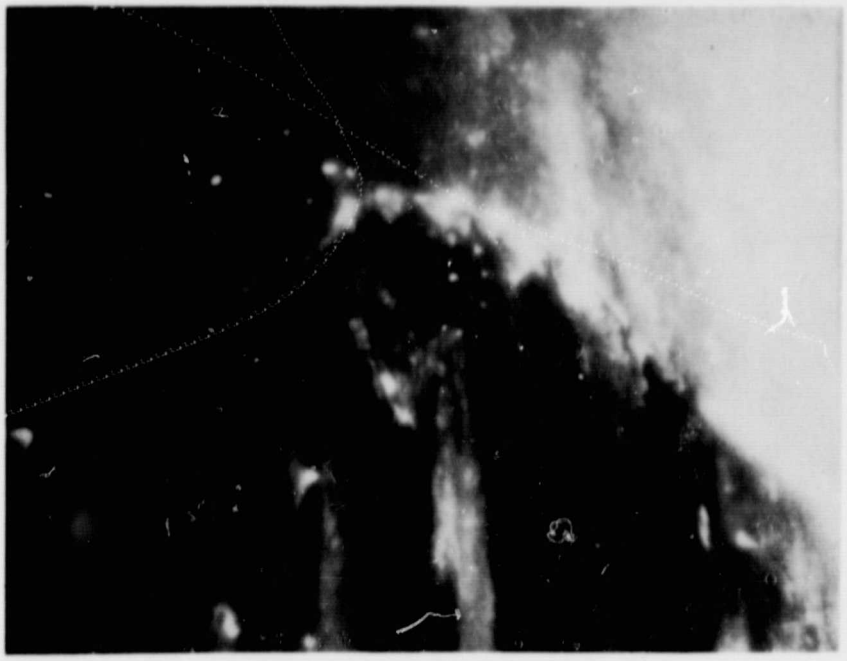

(a)

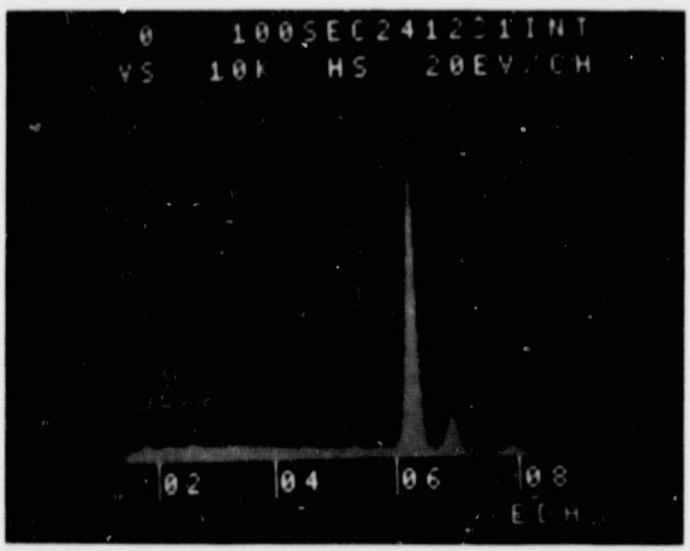

(b)

(a) An SEM micrograph of a ball after hitting the target at 180 m/sec. (X65)

(b) X-ray emission spectrum from upper part of (a).

Figure 14.

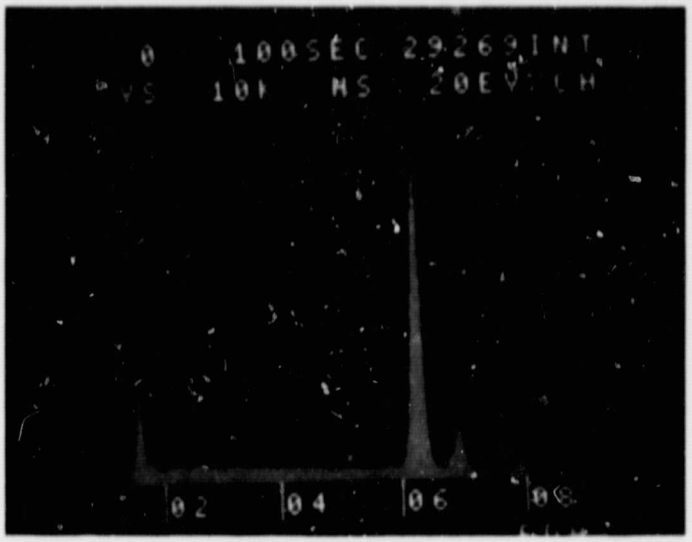

(c)

(c) X-ray emission spectrum from lower part of (a).

Figure 14. - Concluded.

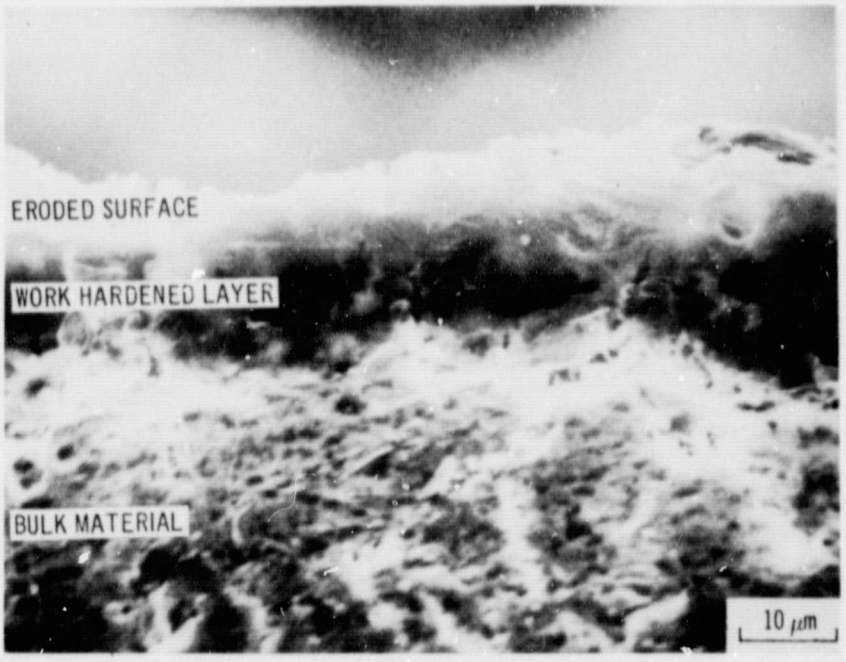

Figure 15. - Cross section at bottom of crater formed by erosion of annealed 6061 aluminum alloy. Etched with a 5% HF (48%), 10% H_2SO_4 (conc.), and 85% H_2O solution.

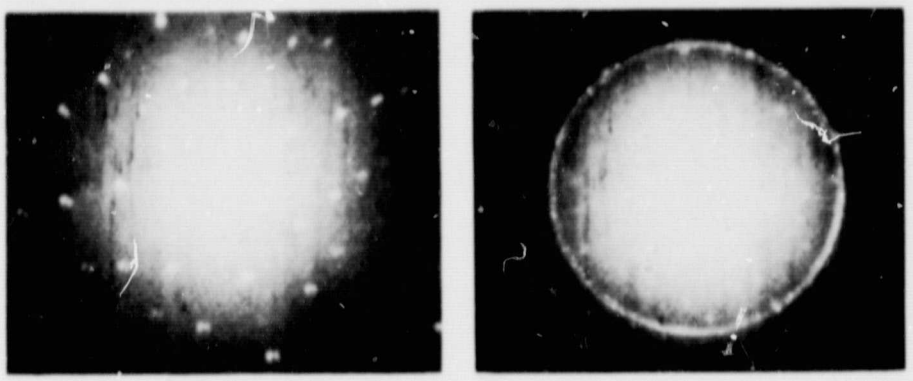

(a) Before erosion. (b) After erosion.

Figure 16. - X-ray diffraction pattern obtained from Al (110) single crystal.

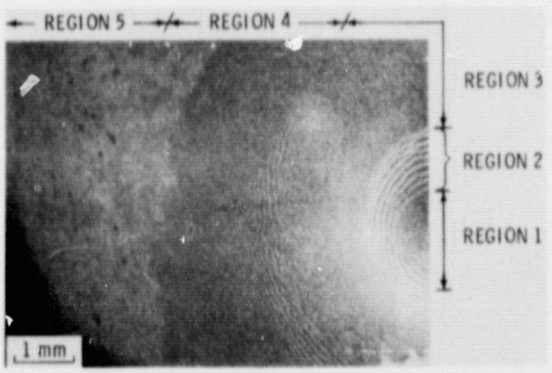

(a) Region 1 - central portion of pit with radial tracks, region 2 - zones containing radial tracks covered by nearly-concentric rings, region 3 - zone with radial tracks only, region 4 - area with circumferential wave patterns, and region 5 - transition zone between eroded and undamaged surfaces.

Figure 17. - SEM photomicrograph of aluminum surface exposed to impingement of glass beads for 20 minutes at 0.41 MPa pressure depicting five different regions.

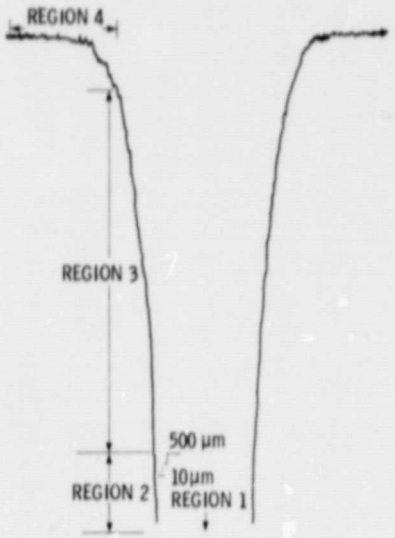

(b) Surface profile of aluminum surface : 0.41 MPa pressure at 20 minutes exposure to glass bead erosion.

Figure 17. - Concluded.

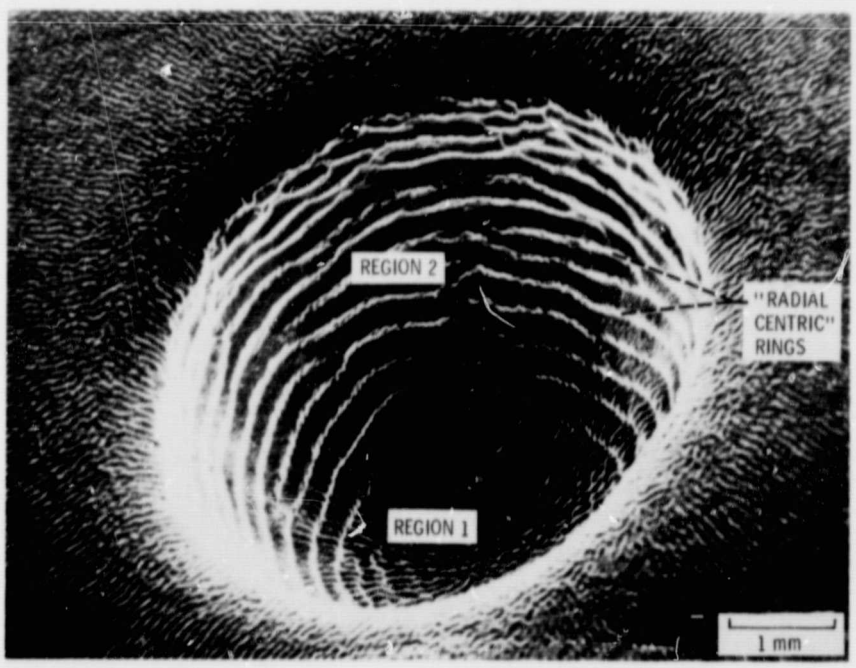

Figure 18. - Scanning electron microscope view of an unusual damage pattern induced in an aluminum alloy by normal impact of spherical glass beads.

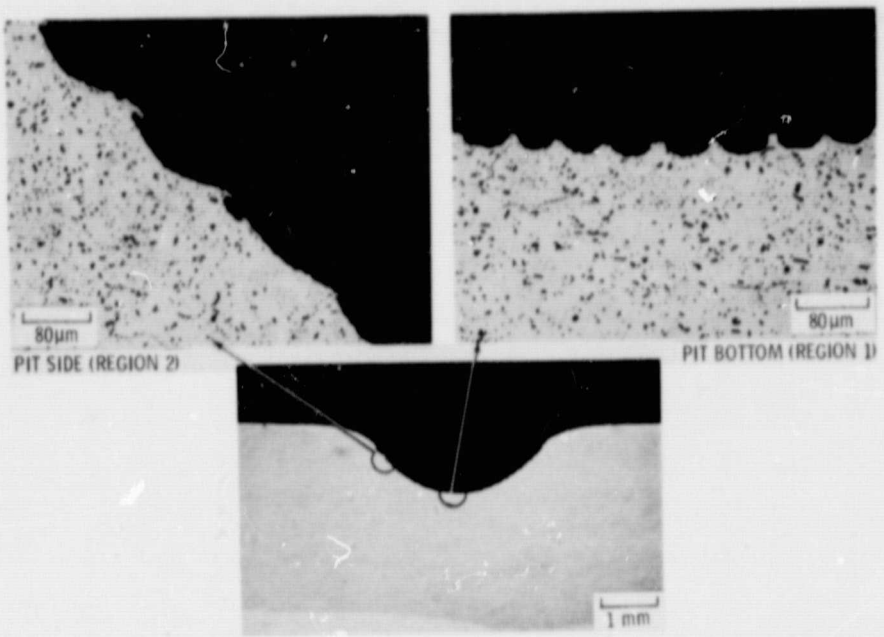

Figure 19. - Cross section through the pit on aluminum at 0.54 MPa pressure and t = 20 minutes.

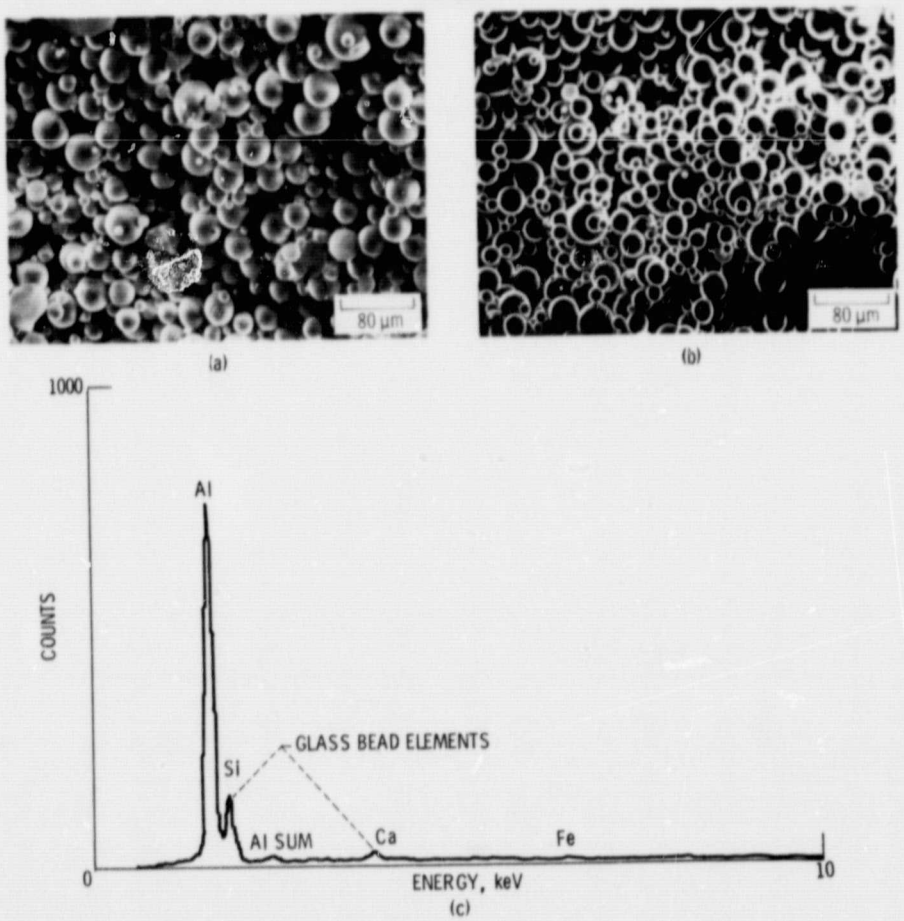

(a) Before impact.

(b) After impact (t = 26 min).

(c) EDS analysis of aluminum specimen surface showing Si and Ca peaks indicating the presence of trapped glass beads on the surface.

Figure 20. - SEM photographs of glass beads before and after impact at 0.54 MPa argon gas pressure.

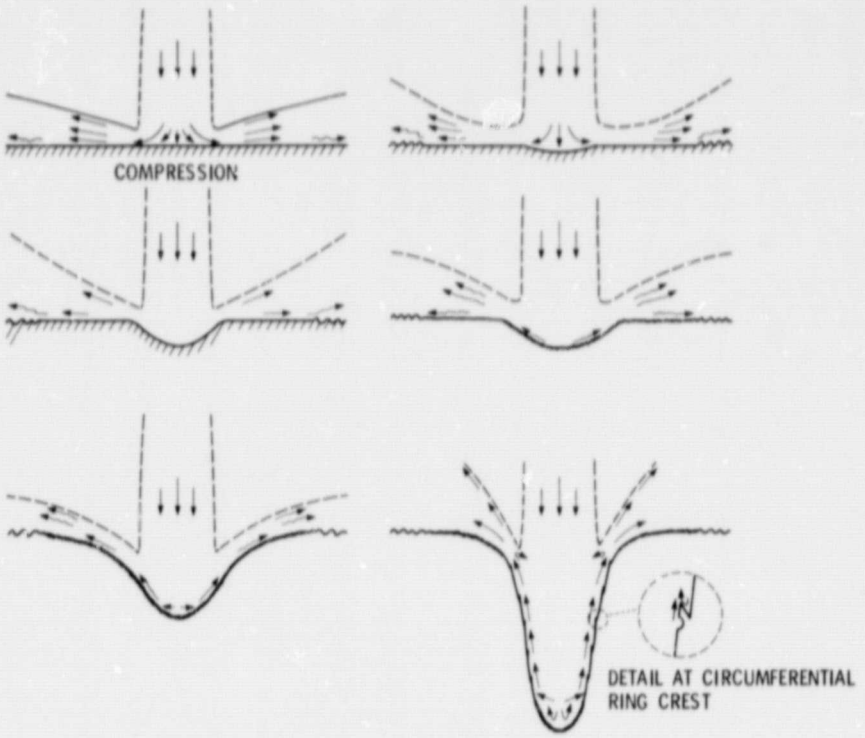

Figure 21. - Sequence of material removal process to explain the morphologic patterns and regions on ductile material surfaces during exposure to glass bead erosion at 90^0 incidence.

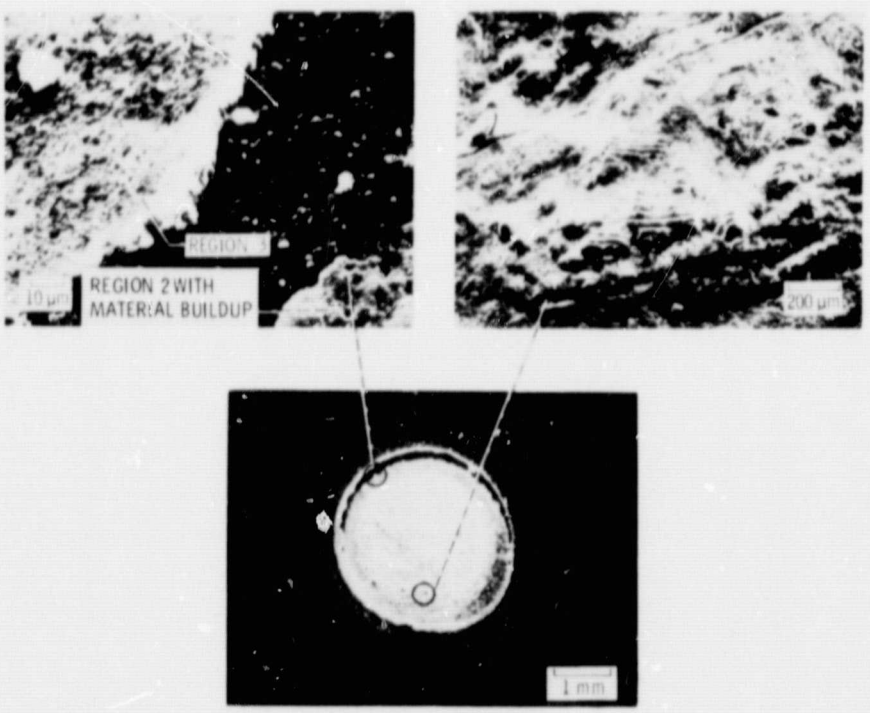

(a) Details of regions 2 and 3.

(b) Material buildup with possible stratification.

(c) 40^0 tilt micrograph of material flow of an eroding pit.

Figure 22. - SEM micrographs of PMMA specimen exposed to glass bead impingement for 15 sec.

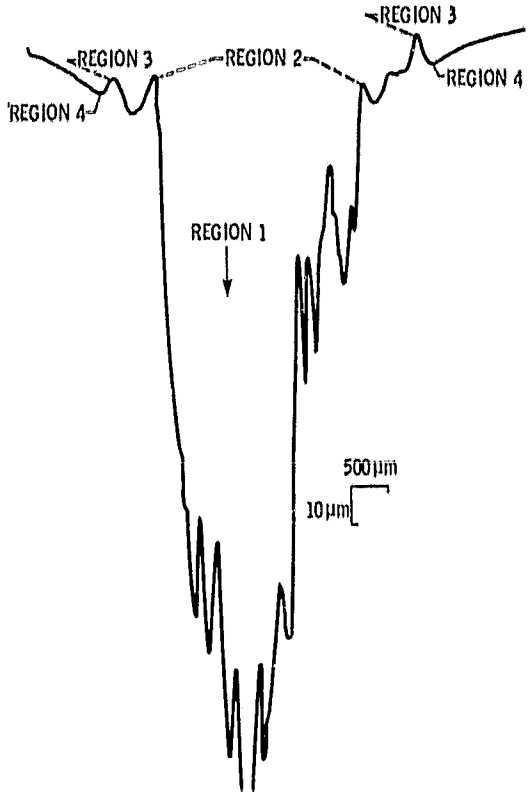

Figure 2 - Surface profile on PMMA surface after 30 seconds exposure to glass bead impingement.